Agilent
Trusted Answers

SZABO SCANDIC
Part of Europa Biosite

Widefield Microscopy as a Screening Tool for Three-Dimensional Cell Culture

Application Compendium

Table of Contents

Introduction

In the body, cells are typically embedded inside ECM or are in direct physical contact with cells from either the same or different lineages.[1] However, most studies in cell biology are performed in conventional two-dimensional (2D) cell cultures systems, which don't replicate the natural microenvironment of the cells.[2] Cellular functions present in tissues are often lost in 2D cell cultures limiting predictive capability of drug testing and impacting cell biological research results. Three-dimensional (3D) cell culture platforms are motivated by the need to work with cellular models that better recapitulate the cellular microenvironment. Cells in a 3D environment behave fundamentally differently from cells in monolayer culture.[3] Many of the observed differences between 2D and 3D culture models are due to differential cell-cell and cell-matrix interactions.[2] Recently, much research has been devoted to developing *in vivo*-like 3D cell culture techniques, which resulted in development of various fabrication methods to facilitate 3D tissue formation.[4] Spheroid culture is one of the most well-characterized models for 3D assays and screening due to its simplicity, reproducibility, and similarity to physiological tissues.[5] The earliest attempts toward development of 3D culture models describe the hanging drop method, where cells spontaneously aggregate in the bottom of a drop after inverting a plate with drops of cell suspension.

Alternatively, spinner flasks enable spontaneous cell aggregation.[6] Another technique, the static liquid overlay technique (LOT), where suspended cells are cultured on a non-adherent substrate, causes cells to aggregate instead of adhering to a surface. More recently, spheroid formation in low-attachment round-bottom plates has become popular as the method offers a simpler workflow and is suitable for high-content imaging.[7] These techniques open doors for new applications of spheroid cultures, such as high-throughput 3D tissue screening for selecting clinically-relevant drugs and the formation of complex, organotypic microtissues.

Critical steps must be taken to facilitate spheroid formation, maintain the highest levels of viability within untreated cells, and ensure that observed effects are solely from treatment of the 3D spheroid culture. These steps include dispensing cells, regular media exchanges, and re-dosing throughout the experiment, particularly for *in vitro* tests lasting weeks. Media exchanges with cell models that do not rely on adherence to labware can be daunting if performed manually, even when performed on a single plate. Multi-channel pipettes must remove and dispense media at an extremely slow rate and care must be taken to keep pipette tips away from the actual spheroids. Automated dispensing using the Agilent BioTek MultiFlo FX multimode dispenser is faster than manual pipetting, yet it can be used to consistently and gently dispense suspended cells into microplates. Additionally, using the Agilent BioTek Automated Media Exchange (AMX) module for the MultiFlo FX minimizes the risk of accidental spheroid aspiration. Spent media is automatically removed and replaced with fresh media only or fresh media containing treatment concentrations.

Different biological readouts from spheroid assays have been described. Common methods include disruption of spheroids and analysis of cell lysates using analytical methods, such as plate reader-based luminescence or fluorescence measurements. However, imaging has advantages over plate reader-based measurements in that no disruption of the spheroids is required and multiple biological readouts are feasible. Therefore, high-content imaging methods have been demonstrated as promising techniques for characterizing the effects of chemical compounds and siRNA libraries on spheroids. Brightfield imaging can be used for morphological characterization of spheroids and fluorescence imaging can be utilized for phenotypic assays that rely on viability dyes, DNA-binding dyes, apoptosis dyes, or other fluorescence markers. Staining a 3D structure may require protocol optimization compared to the 2D equivalent.

In general, the larger and tighter the spheroid, the longer it will take for the labeling reagent to diffuse into the spheroid and longer incubation is required for the staining process to be completed.

If cell permeabilization is required, reagent choice and length of incubation time may need to be considered. In this application compendium, we will introduce 3D-specific reagents that have been optimized for use with spheroids. We have had success using a variety of stains, including primary and secondary conjugated antibodies, with cells cultured in the spheroid microplate. Additionally, pre-labeled or fluorescent-protein-expressing cells can be used prior to seeding in the spheroid microplate to ensure that all cells are labeled as needed for the application.

Because the spheroid is much smaller than the microwell in which it resides, it is critical to understand where the signal is coming from in the well—whether it is a concentrated area or multiple areas within the well. A plate reader is designed to capture as much light as possible from each well, and with spheroids, a pinpoint of light will get lost in the background. Fortunately, with microscopy and image analysis, the field of view can be limited to mostly the spheroid and avoid background radiation coming from the well. Typically, low-magnification imaging is used to include a full spheroid in one image. Light scatter is still limiting effective imaging within the spheroid core even with a large depth of field objective.

The main benefit of the low mag objective is capturing the entire sample width. This approach provides information regarding changes in spheroid diameters or average fluorescence intensities. The thickness of 3D cultures also necessitates the ability to image through the structure. The imaging system must be capable of z-stacking, in which the focal distance can be defined to cover the entire thickness of the 3D system. Using this technique, a series of images are captured at different focus distances; in each image different areas of the sample will be in focus. While none of these images has the sample entirely in focus, they collectively contain all the data required to generate an image that has all parts of the sample in focus. Images of different slices of the z-stack can then be assembled into a composite image using a mathematical algorithm in the Agilent BioTek Gen5 microplate reader and imager software that keeps the in-focus portions of the image and rejects the out-of-focus information. This provides sharper images that can be combined to yield more realistic 3D impressions of the structure of interest. Cellular analysis of 3D cellular structures can also be improved by z-projection. A clear z-projected image of individual cells located in different focal planes of the 3D sample allows for more precise conclusions to be drawn from the experiment being performed.

The goal of this application compendium is to introduce various imaging assays performed with the Agilent BioTek high-content imaging instruments and image analysis software to characterize phenotypic changes in cancer spheroids in response to different compound treatments. In this application compendium, we propose optimized spheroid cell culture protocols for common spheroid cell culture models, such as low-adhesion U-bottom 96- and 384-well plates, Elplasia (microwell plates), and hanging drop method for three common cancer cell lines. Additionally, we introduce an improved workflow for staining that reduces assay time and minimizes variability by recommending suitable reagents and liquid handling systems. We facilitate spheroid image acquisition by using a z-projection algorithm that creates a single composite image from a 3D sample, enabling efficient comparison of different spheroid phenotypes. Automated image analysis is implemented in Gen5 to provide multi-parametric characterization of spheroid morphology and phenotypes. Depending on the assay, Gen5 reports a number of readouts, including morphological characterization (such as spheroid size, area, shape, and volume) and measurement of signal coming from different areas of the spheroid to monitor phenotypic changes, such as spheroid viability, apoptosis, and hypoxia.

Instrumentation

Agilent BioTek Cytation 5 cell imaging multimode reader

Agilent BioTek Cytation 5 is a modular multimode microplate reader combined with an automated digital microscope. Filter- and monochromator-based microplate reading are available and the microscopy module provides up to 60x magnification in fluorescence, brightfield, color brightfield and phase contrast. The instrument can perform fluorescence imaging in up to four channels in a single step. With special emphasis on live-cell assays, Cytation 5 features shaking, temperature control to 65 ºC, CO_2/O_2 gas control and dual injectors for kinetic assays and is controlled by the integrated Gen5 microplate reader and imager software, which also automates image capture, analysis and processing. The instrument was used to kinetically monitor 3D tumoroid activity over the incubation period.

Agilent BioTek MultiFlo FX multimode dispenser

The Agilent BioTek MultiFlo FX multimode dispenser combines multiple dispensers in one compact unit, thus reducing overall instrument costs, saving processing time, and simplifying the process. The MultiFlo FX is a modular, upgradable reagent dispenser that can have as many as two peri-pump (8-tube dispensers), two syringe pump dispensers and a strip washer. The syringe and washer manifolds can be configured for plate densities from 6- to 384-well. For use with cell-based assays, the MultiFlo FX can be placed in a laminar flow hood for sterile operation. In the assays detailed in this application compendium, the MultiFlo FX was used to dispense cells and media, as well as reagents to assay wells. The MultiFlo FX was equipped with the Agilent BioTek Automated Media Exchange (AMX) module.

Agilent BioTek Automated Media Exchange (AMX) module

Spheroid culture media exchanges can be accomplished through use of the Agilent BioTek Automated Media Exchange (AMX) module, which consists of two unique, modified peristaltic pump cassettes with eight stainless steel tube aspirate and dispense heads. The cassette tubing is fed through the peristaltic pumps of the MultiFlo FX and into media bottles or tubes. Software allows the pumps to run slowly and gently so as to not disturb the spheroids during aspirate or dispense procedures. Each cassette is fully autoclavable, enabling sterile processing.

Agilent BioTek BioSpa 8 automated incubator

The Agilent BioTek BioSpa 8 automated incubator links Agilent BioTek readers or imagers together with Agilent BioTek washers and dispensers for full workflow automation of up to eight microplates. Temperature, CO_2/O_2 and humidity levels are controlled and monitored through the Agilent BioTek BioSpa software to maintain an ideal environment for cell cultures during all experimental stages. Test plates were incubated in the BioSpa to maintain proper atmospheric conditions for a period of seven days and automatically transferred to the Cytation 5 every twelve hours for brightfield and fluorescence imaging.

3D Imaging Applications for Morphological and Phenotypic Characterization of 3D Cancer Spheroids

Brightfield and fluorescence imaging using 3D PrimeSurface ultra-low attachment microplates

Assay introduction

Developing uniform spheroids becomes important, as it forms the basis for robust and reliable assays. S-BIO PrimeSurface culture ware are ultra-low attachment (ULA) dishes and plates that promote scaffold-free, self-assembly spheroid formation. The plates are pre-coated with a proprietary hydrophilic polymer that enables spontaneous spheroid formation of uniform size. Prime Surface 96 and 384 ULA plates have good optical clarity, making them highly suitable for brightfield and fluorescent imaging. Imaging technologies, such as the Agilent BioTek cell imaging multimode readers, allow researchers to study not only spheroid proliferation through brightfield imaging, but also phenotypic events using fluorescent probes and fluorescence imaging. Incorporation of z-stacking and projection techniques in the Gen5 microplate reader and imager software create in-focus images of spheroidal cells, allowing accurate, robust, and repeatable determination of the effect of test molecules or conditions. In this application compendium, we present data generated with the Agilent BioTek Cytation 5 cell imaging multimode reader using PrimeSurface ULA plates to develop simple robust spheroid assays for brightfield and fluorescence imaging.

Method summary

HT-1080 cells were seeded in 96- and 384-well PrimeSurface U-bottom microplates at different concentrations ranging between 10,000 and 50 cells per well. The microplates were incubated for 48 hours to allow the cells to aggregate into spheroids. After spheroid formation, cells were treated with Camptothecin and plates were then incubated for an additional 24 hours to induce necrosis within the treated spheroidal cells. The following day, the media was replaced with 1x CellTox Green (Promega Corporation, Madison, WI) necrotic cell stains and cells were incubated for 5 hours to allow fluorescent probe penetration into the cells. As the cells within the spheroids exist within a range of z-planes, z-stack images were captured above and below the focal plane to ensure cells were imaged at the proper z-height. 3D image processing was applied to create a z-projection of the images in the z-stack. A cellular analysis step was then applied to projected images according to optimized object selection criteria to identify untreated variable-sized spheroids in the brightfield channel. An additional cellular analysis step was performed on the treated spheroids to determine the extent of necrotic activity induced by the Camptothecin treatment.

Results summary

Brightfield imaging of formed spheroids

Visual analysis of the z-projected images reveals that HT-1080 cells are able to form tight spheroids within the 96-well U-bottom plates. It is also evident that the z-stacking and projection method used by the Gen5 microplate reader and imager software creates accurate, in-focus spheroidal images, regardless of size. Gen5 accurately identifies each spheroid by the accurate placement of primary masks in brightfield images, which is necessary for area and diameter measurements (Figure 1A-C). Using the two metrics, a volume calculation can be made. Spheroid volume analysis was performed in both 96- and 384-well formats. The precision and linearity of spheroid volume analysis as a function of cell seeding density are demonstrated in Figure 1D in both 96- and 384-well PrimeSurface plates.

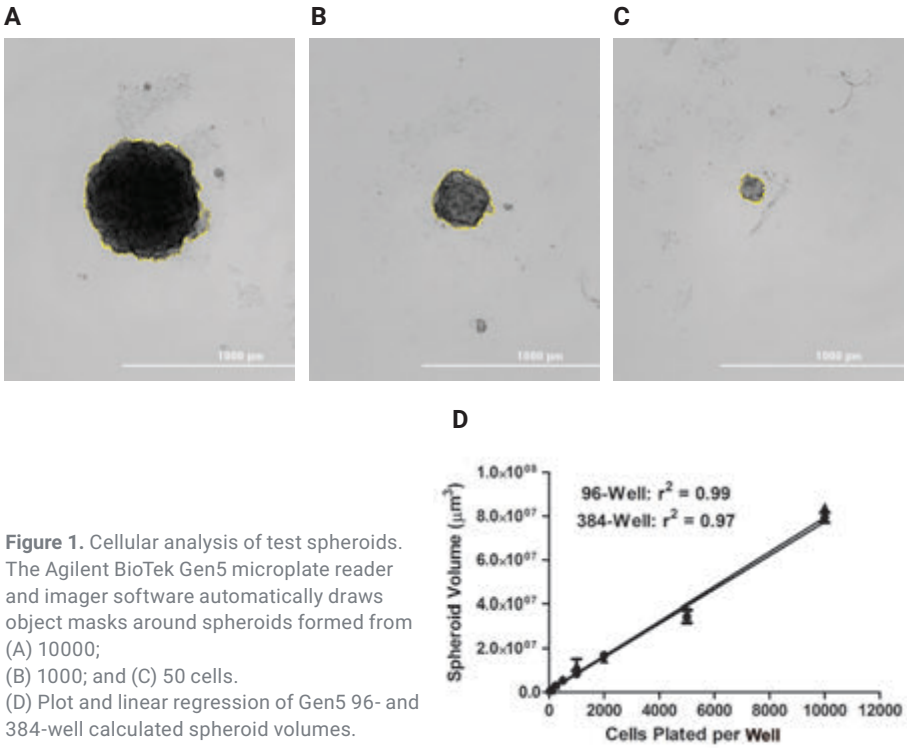

Figure 1. Cellular analysis of test spheroids. The Agilent BioTek Gen5 microplate reader and imager software automatically draws object masks around spheroids formed from (A) 10000;
(B) 1000; and (C) 50 cells.
(D) Plot and linear regression of Gen5 96- and 384-well calculated spheroid volumes.

Fluorescent imaging of necrotic cell induction within spheroids

Fluorescent images, captured in the GFP channel, were subsequently analyzed to determine the level of necrotic cell induction caused by Camptothecin. After masking each spheroid in the Brightfield channel, Gen5 calculates the area covered solely by necrotic cells within each test spheroid (Figure 1A-C). We confirmed in the analysis that background autofluorescence from the clear wall is minimized due to the geometry of these U-bottom plates, allowing for an easily distinguishable change in signal from affected cells. When the necrotic cell area was divided by the total cell area, a normalized affected cell percent coverage area was created, which accounted for variances in area between the treated 1000 cell spheroids. The values were then plotted in terms of the concentration of Camptothecin used for treatment (Figure 2D). It is apparent from the Brightfield images that the background signal generated from the bottom of the plate is relatively bright and very uniform in intensity.

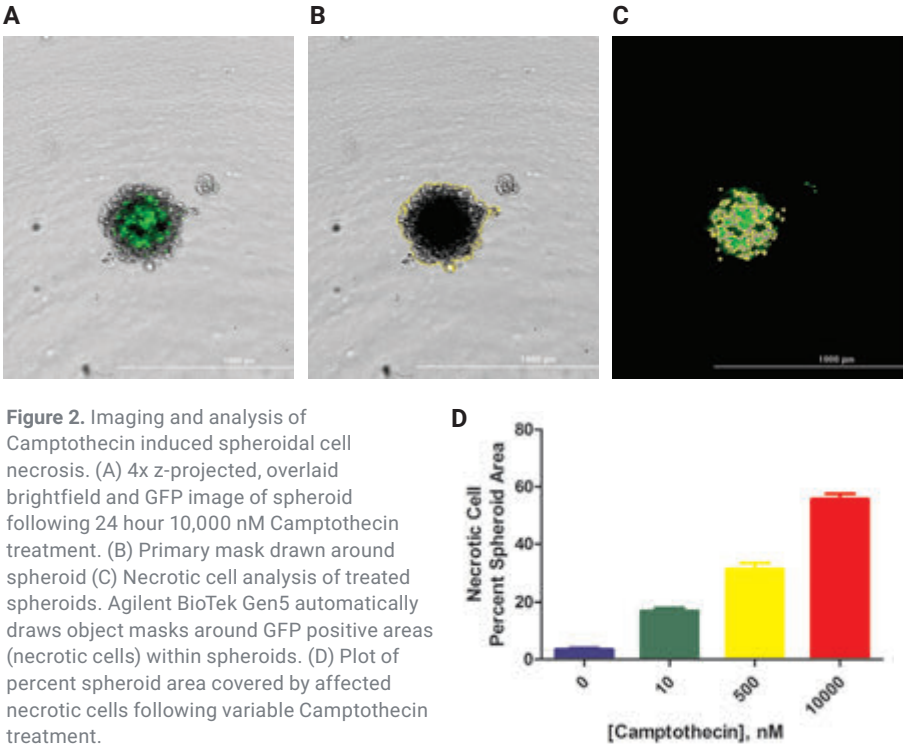

Figure 2. Imaging and analysis of Camptothecin induced spheroidal cell necrosis. (A) 4x z-projected, overlaid brightfield and GFP image of spheroid following 24 hour 10,000 nM Camptothecin treatment. (B) Primary mask drawn around spheroid (C) Necrotic cell analysis of treated spheroids. Agilent BioTek Gen5 automatically draws object masks around GFP positive areas (necrotic cells) within spheroids. (D) Plot of percent spheroid area covered by affected necrotic cells following variable Camptothecin treatment.

Recent publications using Agilent BioTek microscopes for monitoring spheroid formation

1. Dong, G. et al. "Serum-Free Culture System for Spontaneous Human Mesenchymal Stem Cell Spheroid Formation". *Stem Cells Int. 2019*, **2019**.
2. de la Cruz Bonilla, M., Stemler, K. M., Taniguchi, C. M. & Piwnica-Worms, H. "Stem cell enriched-epithelial spheroid cultures for rapidly assaying small intestinal radioprotectors and radiosensitizers *in vitro*". *Sci. Rep. 8, 2–9,* **2018**.

Utilizing automated imaging and advanced 3D cell culture techniques to quantify apoptosis activity

Assay summary and reagents

Apoptosis, or programmed cell death, is essential to normal development and homeostasis of all multicellular organisms, and is, in fact, a key research tool in the fight against cancer. Yet a challenge remains when using 2D cultured tumor cells as they may not respond to cancer therapeutics/compounds in the same fashion as they would *in vivo*. Three-dimensional (3D) methods provide more physiological conditions for the cells, which are beneficial for investigating mechanistic processes and drug resistance in tumor cells. This application describes the utility of a novel 3D spheroid cell culture model, Elplasia, used to elucidate the apoptotic potential of Doxorubicin HCl and Oridonin against HT-1080 fibrosarcoma cells and HCT116 colorectal carcinoma cells. The microwell geometry aids spheroid formation in the center of each well, while the optically clear round bottom allows cellular imaging and the opaque body prevents cross-talk. Spheroid growth and induced apoptosis levels within the spheroids were then quantified, using a cell imaging multimode reader.

A

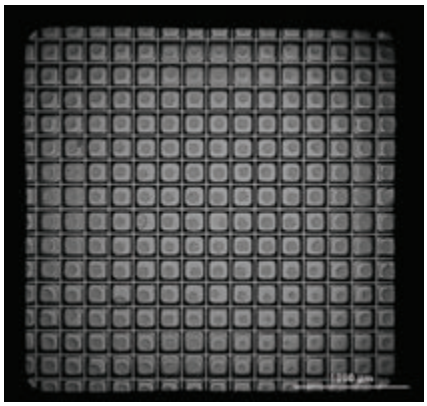

B

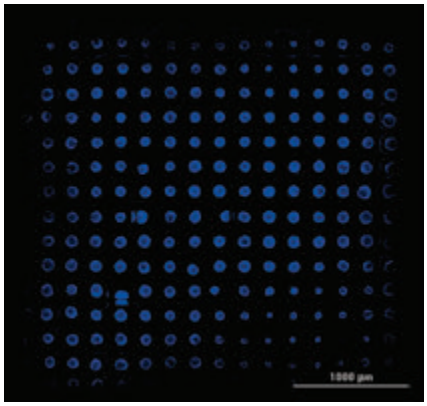

Figure 3. Microspace imaging at 4x magnification. (A) Stitched 2x2 montage images of HCT116 spheroids in a well microspace. (B) DAPI channel imaging of spheroid location.

Method summary

HCT116 and HT 1080 cells were harvested, 50 µL of suspended cells were added to separate test wells in the Elplasia 384-well microplate, for a total of approximately 50 cells per microspace. The plates were incubated for 48 hours to allow the cells to aggregate. Serial titrations of Doxorubicin and Oridonin were created, ranging from 20-0 µM (2x), using 1:4 dilutions, in medium containing Hoechst 33342 and the Kinetic Apoptosis Reagent, pSIVA-IANDB, contained within the Kinetic Apoptosis Kit (Abcam, Cambridge, UK). Phosphatidylserine is a cytosolic-facing cell membrane component and its exposure on a cell's extracellular surface, either persistently or transiently, is an indicator of early apoptosis. The cell membrane impermeant fluorescent probe, pSIVA-IANDB binds to phosphatidylserine, creating a strong green fluorescent signal to allow apoptosis monitoring over time.

After spheroid creation, 25 µL of medium was removed from each well, and replaced with an equal amount of either the doxorubicin or oridonin compound titration. For spheroid apoptosis analysis, the plates were placed into Cytation 5, and kinetic imaging was performed every four hours over a 48-hour period. A 4x objective was used to image the entire well using the brightfield imaging channel, with a 2x2 image montage incorporated to visualize the entire well. The same objective was used, along with DAPI and GFP imaging channels, to image all spheroids, and apoptotic spheroids, respectively.

Results summary

HCT116 spheroid proliferation and location within the microspace was confirmed using Cytation 5 and Gen5 microplate reader and imager software. Using brightfield imaging, four images were captured in a 2x2 configuration to cover the well. The images were stitched together, using Gen5 software, to create a final, single image of all the microspaces in a well (Figure 3A), while staining with Hoechst 33342 allowed identification of spheroid using the DAPI channel (Figure 3B). Using pSIVA-IANBD, HCT116 and HT 1080, spheroid apoptotic activity was tracked over the compound concentrations tested. High apoptotic activity was observed when spheriods were treated with 400 nM doxorubicin, for 48 hours, represented by high levels of green fluorescence (Figure 4B).

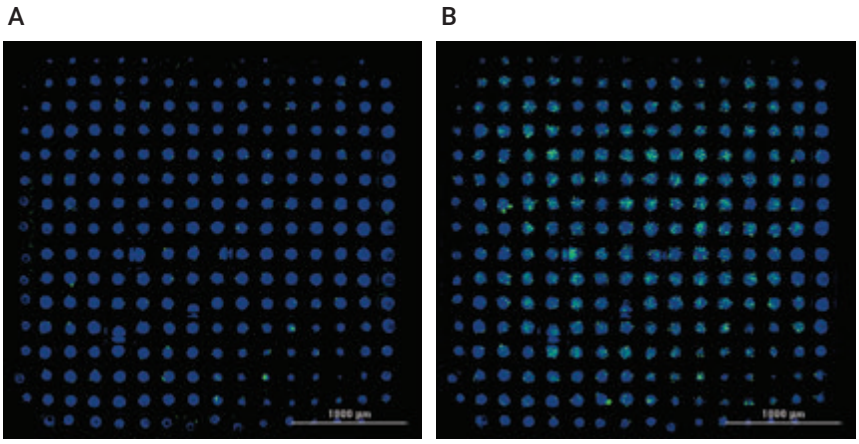

Figure 4. Apoptotic activity in HT-1080 cells treated with 400 nM doxorubicin. 4x DAPI and GFP channel imaging (A) 24 hours post-treatment and (B) 48 hours post treatment.

Using cellular analysis features in Gen5, individual spheroids were automatically detected in each image by optimizing object selection criteria such as the intensity threshold and object size range. Non-spherical objects were excluded using size and circularity sub-population criteria outlined in Table 1.

Table 1. Agilent BioTek Gen5 microplate reader and imager software fluorescent spheroid analysis primary, advanced, and sub-population parameters.

Spheroid Primary Cellular Analysis Parameters	
Channel	DAPI
Threshold	Auto-2
Background	Dark
Minimum Object Size	25 µm
Maximum Object Size	150 µm
Fill Holes in Masks	Checked
Split Touching Objects	Checked
Analyze Entire Image	Checked
Include Primary Edge Objects	Unchecked

(Continued)

Advanced Options	
Evaluate Background On	5% of lowest pixels
Image Smoothing Strength	0
Background Flattening Size	1000 µm
True Spheroid Sub-population Parameters	
Size	>85 µm
Circularity	>0.4
Apoptotic Spheroid Sub-population Parameters	
Size	>85 µm
Circularity	>0.4
Mean GFP	>6000

Finally, a second sub-population filter was applied to identify the number of apoptotic spheroids by setting the threshold for the mean GFP signal intensity (Figure 5A-C). It is important to note that cellular analysis parameters may vary depending on cell type, so parameter optimization should always be performed on multiple wells to confirm the accuracy. Our results show that the predicted drug efficacy can be skewed by inconsistency of the spheroid count in each well. To account for such anomalies, we reported apoptotic spheroid percentage per well as a readout. The value was calculated by dividing apoptotic spheroid numbers by the total identified actual spheroids per well. The resulting percent apoptotic spheroid kinetic graphs can be used to ascertain differences between compound effects on 3D spheroids.

As Figure 5 suggests, the compounds exhibit a stronger apoptotic effect on HT1080 spheroids as witnessed by the rapid rise in apoptotic spheroid percentage at low compound concentrations. Apoptotic activity then decreases at compound concentrations above 1000 nM, most likely due to the cells within each spheroid becoming necrotic. HCT116 spheroids are more resistant to the compounds, as higher compound concentrations are needed to elicit an apoptotic response.

The combined results illustrate that specific phenotypic apoptotic effects are able to be detected from individual cell-type (e.g. primary cell, stem cell, and cancer cell line) and drug combinations using cellular imaging and the Elplasia spheroid microplates.

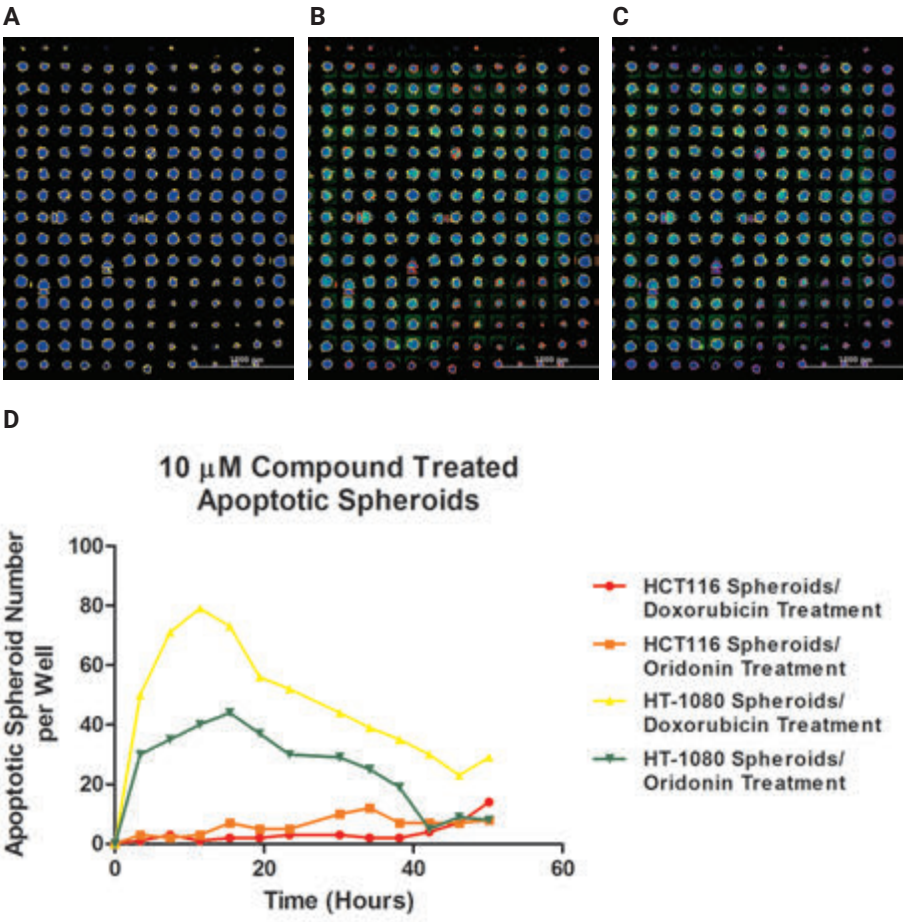

Figure 5. Cellular analysis procedure to determine apoptotic spheroid number per well. (A) The Agilent BioTek Gen5 microplate reader and imager software masks automatically drawn around objects meeting primary and advanced cellular analysis criteria using DAPI channel captured Hoechst 33342 signal; (B) red object masks indicating eliminated artifacts and spheroids not meeting minimal size and circularity sub-population requirements; and (C) purple object masks denoting objects not meeting initial sub-population criteria in addition to not meeting apoptotic spheroid criteria. (D) Kinetic graph showing percent apoptotic HCT116 or HT-1080 spheroids treated with a single 10 µM concentration of doxorubicin or oridonin.

Recent publications using Agilent BioTek microscopes for measuring apoptosis in spheroids

1. Darrigues, E. et al. "Tracking Gold Nanorods' Interaction with Large 3D Pancreatic-Stromal Tumor Spheroids by Multimodal Imaging: Fluorescence, Photoacoustic, and Photothermal Microscopies". *Sci. Rep. 10, 3362,* **2020**.
2. Nanayakkara, A. K. et al. "Targeted inhibitors of P-glycoprotein increase chemotherapeutic-induced mortality of multidrug resistant tumor cells". *Sci. Rep. 8, 1–18,* **2018**.

3D Spheroid-based tumor invasion assay

Assay introduction

Oncology drug discovery has been met with multiple challenges over the years. The advancement of novel methods that focus on the inhibition of the invasive phenotype of metastasis offers greater potential for meaningful intervention, particularly due to the high mortality rate of the patients who die from cancer metastasis. To reduce the relevant attrition rate during drug development, 3D *in vitro* cell models used in early drug discovery should mimic the complex metastatic process as closely as possible. Tumors *in vivo* exist as a three-dimensional (3D) mass of multiple cell types, including cancer and stromal cells. Therefore, incorporating a 3D spheroid type cellular structure that includes co-cultured cell types forming a tumoroid provides a more predictive model than the use of individual cancer cells seeded in microplates.

To capture the cell invasion process, long-term kinetic experiments need to be performed. Thus, environmental control of the assay is needed such that the cell viability of the spheroid is maintained over this long period and putative drug effects can be properly assessed. Finally, the only suitable readout for monitoring tumor invasion is microscopy due to the small size of the spheroid. To be effective in drug discovery, the microscope must have automated image capture, processing and analysis to be able to cope with the multiple assay conditions, compounds tested and kinetic images taken.

This work will demonstrate a procedure for the generation of 3D spheroidal tumoroid structures, creation of a suitable invasion matrix, automated kinetic image-based monitoring, and cellular analysis of captured z-stacked images of tumor invasion.

U-87 and LN-229 glioblastoma multiforme (GBM) cell lines were used in this study, as they have demonstrated phenotypic differences and metastatic ability. Both cell types were co-cultured with fibroblasts to create 3D tumoroids more closely representing *in vivo* tumor conditions and allowed to invade through a protein matrix. 17-allylamino- 17-demethoxygeldanamycin (17-AAG), known to inhibit the function of heat shock protein 90 (Hsp90), a chaperone protein that stabilizes proteins required for tumor growth, was used here to inhibit potential tumor invasion. Quantification of kinetic captured images was used to characterize the invading potential of inhibited and uninhibited tumoroid cultures.

Method summary

Tumor invasion assay preparation

A mixed cell suspension was prepared by combining U-87 and fibroblast cells in a final concentration of $2.5x10^4$ cells/mL for each cell type in complete medium. After dispensing 100 µL of cell suspension into appropriate microplate wells, the microplate was incubated for forty-eight hours to allow cells to aggregate into tumoroids. This process was repeated for LN-229 cells stained with CellTracker Deep Red dye (ThermoFisher Scientific, Waltham, MA.) and fibroblast cells at the same concentrations and volumes. Upon completion of tumoroid formation, 70 µL of complete medium was robotically removed from each well and the tumoroid plate placed on ice in a refrigerator for five minutes to cool the cells. The Matrigel matrix was then thawed on ice. Different concentrations of 17-AAG ranging between $0\text{-}2*10^4$ nM was prepared either in invasion media or Matrigel matrix. Afterwards, 70 µL of Matrigel matrix plus titrated compound were added to each well containing tumoroids, then overlaid with 100 µL of invasion media containing titrated compound. The microplate was centrifuged at 300 × g for five minutes and incubated for one hour to initiate gel formation.

Tumor invasion imaging and analysis

After gel formation was complete, the microplate was transferred to the BioSpa 8 automated incubator, where the software was programmed such that the microplate was automatically transferred to Cytation 5 for brightfield and fluorescent imaging of the wells every twelve hours over the seven day incubation period. Table 2 lists the settings used to perform automated image capture of each sample well. We used a combination of image montage and z-stack to capture the full area and depth of the tumoroid tissue.

Table 2. Automated 3D tumoroid invasion imaging parameters.

Imaging Parameters	
Brightfield Imaging Channel	Complete 3D invading structure
GFP Imaging Channel	U-87 cells expressing GFP
RFP Imaging Channel	Fibroblasts expressing RFP
CY5 Imaging Channel	LN-229 cells stained with CellTracker Deep Red Dye
Objective	4x
Montage	3 row by 2 column
Montage Overlap	Auto for stitching
Z-Stack	20 slices
Z-Stack Step Size	53.8 µm (default for 4x objective)

First, we applied image stitching to merge individual tiles together (Table 3A).

Table 3A. Image stitching parameters.

Imaging Stitching Parameters	
Registration Channel	Brightfield
Fusion Method	Linear blend
Crop Stitched Image to Remove Black Rectangles on the Borders	Checked
Downsize Final Image	Checked (52.62%)

A single image projection was created from the 20-slice stitched z-stack (Table 3B).

Table 3B. Image Z-projection parameters.

Imaging Z-Projection Parameters	
Channel 1	Stitched[Brightfield]
Method	Focus stacking
Size of Maximum Filter	11 px
Z-Slices Included	1-20
Channels 2-4	Stitched[GFP], Stitched[RFP], Stitched[CY5]
Method (Channels 2-4)	Use settings of channel 1

The focus stacking method was chosen, which automatically selects the most in focus pixel from each image in the stack for inclusion in the final projection. This allows for the most accurate analysis to be carried out on each invading tumoroid at each timepoint. To quantify the tumor invasion, primary mask cellular analysis criteria were applied using the brightfield channel to automatically place object masks around the entire invading structure in each final image (Table 4A).

Secondary mask cellular analysis criteria were also applied to place an additional mask around non-invasive cells remaining within the original spherical tumoroid structure (Table 4B).

Table 4A. Primary mask analysis parameters.

Primary Cellular Analysis Parameters	
Channel	ZProj[Stitched[Brightfield]]
Threshold	25,000
Background	Light
Split Touching Objects	Unchecked
Fill Holes in Masks	Checked
Minimum Object Size	300 µm
Maximum Object Size	2000 µm
Include Primary Edge Objects	Checked
Analyze Entire Image	Checked
Advanced Detection Options	
Rolling Ball Diameter	2000
Image Smoothing Strength	0
Evaluate Background On	5% of lowest pixels
Analysis Metric	
Metric of Interest	Object area

Table 4B. Secondary mask analysis parameters.

Secondary Cellular Analysis Parameters	
Channel	ZProj[Stitched[Brightfield]]
Measure Within a Secondary Mask	Include primary mask
Reduce Primary Mask	1 µm
Threshold	12,000
Smooth	7
Fill Holes in Mask	Unchecked
Analysis Metric	
Metric of Interest	Object Area_2[ZProj[Stitched[Brightfield]]]

Assay results

During the seven-day incubation period, uninhibited U-87/fibroblast tumoroids continued to increase in size, as well as invade into the protein matrix. To ensure that the entire invading structure, including invadopodia, was captured in the x-, y- and z- axes, multiple images were automatically taken across a range of z-heights in a montage format (Table 2). In addition to brightfield imaging, montage tiles and z-stacked layers were also captured using the GFP and RFP channels.

Overlaying images tracks invasion of the entire structure (Figure 6). By viewing the fluorescent signal emitted by each co-cultured cell type, we compared the migratory behavior of two tested cell types. In the case of the U-87/fibroblast model, the brightfield image demonstrates extensive invadopodia extending out from the original propagating tumoroid (Figure 7A). From the GFP image in Figure 4B, it is evident that GFP-expressing U-87 cells follow invadopodia invasion into the matrix. This contrasts to the RFP image in Figure 4C, confirming that RFP-expressing fibroblasts exhibit little to no migratory ability within this experimental model.

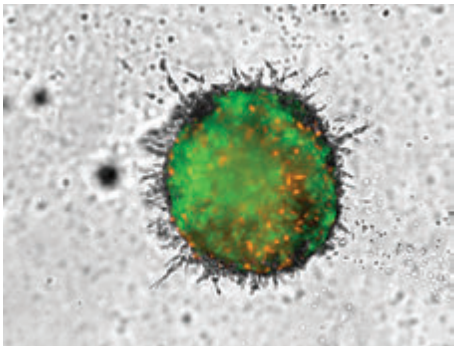

Figure 6. Brightfield and fluorescent overlaid z-projected image of U-87/fibroblast co-cultured cell model.

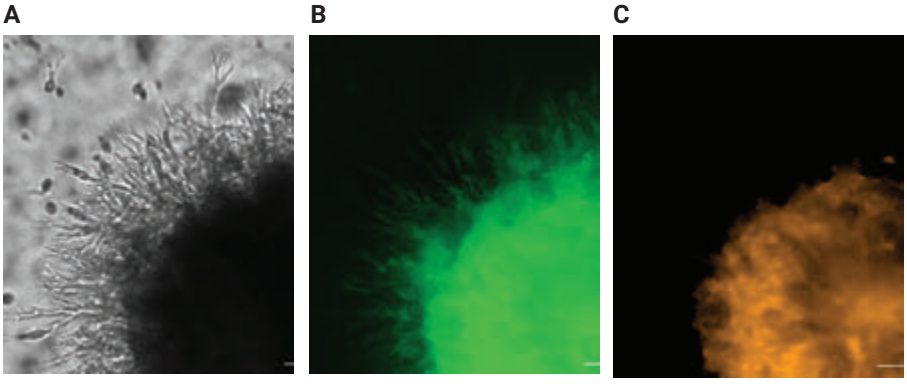

Figure 7. Confirmation of invasion by individual cell types. (A) total tumoroid invasion via overlaid GFP, RFP and brightfield channels. Individual cellular invasion by (B) GFP-expressing U-87 cells; or (C) RFP-expressing fibroblast cells. Digitally zoomed 4x images, 2x3 montage, 20-plane z-stack.

Kinetic monitoring of tumor invasion

Tumor invasion was monitored by capturing images every 12 hours to observe phenotypic changes in the U-87/ fibroblast co-cultured tumoroids after treating with varying concentrations of 17-AAG. We observed a highly invasive phenotype for untreated tumors, represented by an increase in the size of the tumoroid body, as well as a dramatic increase in invadopodia formation (Figure 8A). We repeated the kinetic imaging for LN-229/fibroblast tumoroid and compared the differences in growth and invadopodia production between GBM cell types as an invasive cell model (U-87) and cells with less invasive ability (LN-229) (Figure 8A). When comparing kinetic brightfield images from the two co-cultured cell types, it is evident that LN-229/fibroblast tumoroids propagate over time, as seen by the increase in spheroid size (Figure 9), but do not exhibit the invasive properties clearly demonstrated by U-87/fibroblast tumoroids over the same incubation period (Figure 8B).

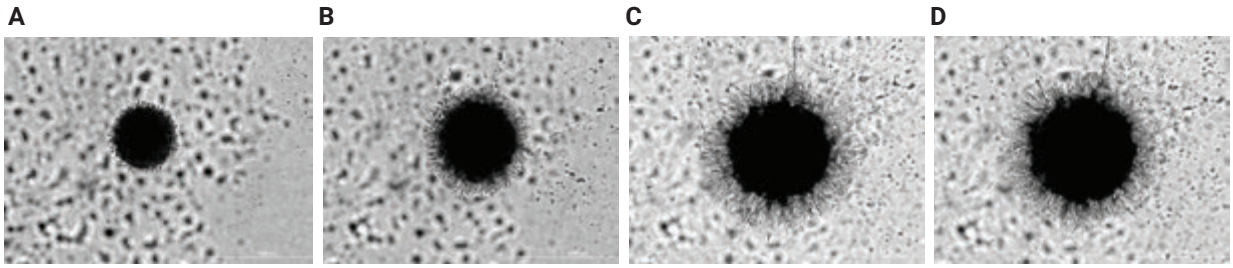

Figure 8. Analysis of tumoroid invasive potential over time, 4x brightfield images, 2x3 montage, 20-plane z-stack. (A) 0 hours; (B) 48 hours; (C) 120 hours; (D) 168 hours for a) U-87/fibroblast and b) LN-229/fibroblast cell mixture.

Changes in the complete 3D structure were observed using the overlaid brightfield and fluorescent images (Figure 9A), while individual LN-229 or fibroblast invasion were monitored by signal captured with the individual CY5 or RFP channels, respectively (Figure 9B and C).

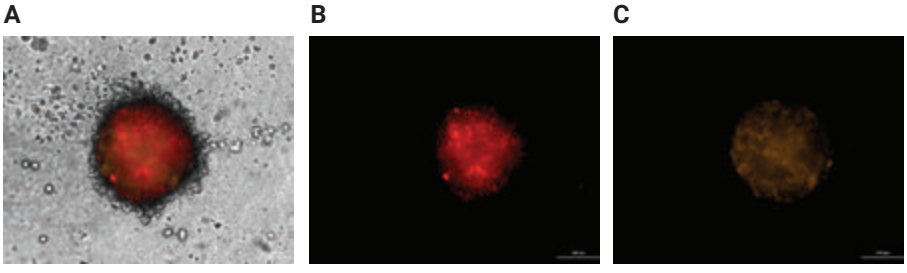

Figure 9. Imaging of LN-229/fibroblast co-cultured cell model. (A) Total tumoroid invasion via overlaid CY5, RFP and brightfield channels. Individual cellular invasion by (B) CellTracker Deep Red stained LN- 229 cells; or (C) RFP-expressing fibroblast cells. Digitally zoomed 4x images, 2x3 montage, 20-plane z-stack.

Automated cellular analysis of tumoroid invasion using Gen5

Quantification of the extent of invasion was carried out using the stitched, z-projected brightfield images. We used BF images and object selection criteria listed in Table 4A to place detailed object masks around the invaded 3D tumor structure (Figure 10). The area covered by the entire tumoroid for each captured image over time was then calculated. Values from subsequent time points were then divided by the area value calculated at time 0 for the specific tumoroid to normalize results and account for variability in tumoroid size following cell dispensing and aggregation. Area ratios were then plotted (y-axis) with regards to time (x-axis) (Figure 11). From the results seen in Figure 11, it is apparent that both U-87/fibroblast and LN-229/fibroblast tumoroids propagate within the Matrigel matrix when unimpeded over the seven-day incubation period. It can also be seen that the compound 17-AAG is able to limit, or even completely stop, tumoroid growth in a dose-dependent manner, as expected. What is also clear from the total area ratio graphs is the increased rate of growth for the complete 3D structure exhibited by U-87/fibroblast tumoroids compared to those where LN-229 cells are co-cultured with fibroblasts. Increases in the area covered by the entire tumoroid are approximately 2x over time for tumoroids cultured with U-87 cells (ratio: 4.4) compared to those cultured with LN-229 cells (ratio: 2.4).

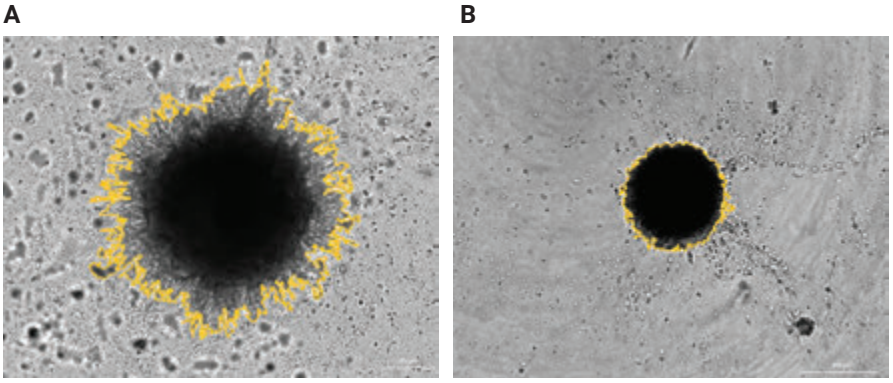

Figure 10. Invading tumoroid object masking. Zoomed 4x brightfield images of U-87/fibroblast tumoroids, 2x3 montage, 20-plane z-stack. (A) 0 µM 17-AAG treatment; and (B) 10 µM 17-AAG treatment. Primary masks around cells and invadopodia.

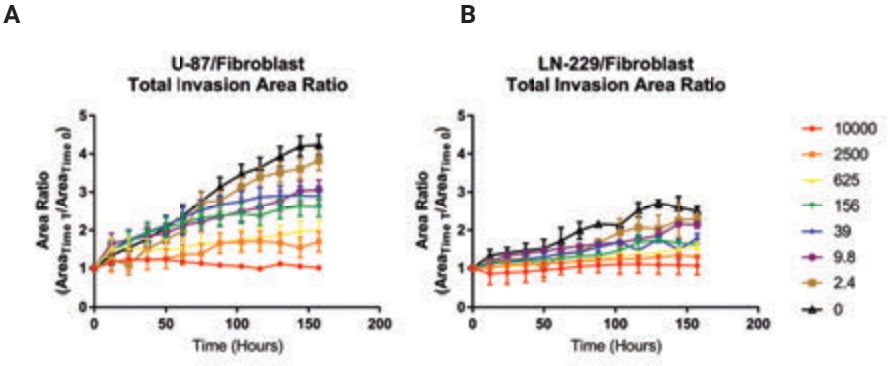

Figure 11. Kinetic total tumoroid area ratios. Area ratios plotted for (A) U-87/fibroblast tumoroids, or (B) LN-229/ fibroblast tumoroids following 0-7 day treatments with 17- AAG concentrations ranging from 10,000 to 0 nM.

Gen5 image prime-based cellular analysis of tumoroid invasion

A second cellular analysis was also performed using the primary and secondary cellular analysis capabilities available in Agilent BioTek Gen5 Image Prime, and the criteria listed in Table 4B to measure the area solely covered by non-invading cells within the tumoroid. In order to determine the metastatic ability of 3D *in vitro* models, both for control and treatment wells, it is important to be able to distinguish between the area covered by cells within the original tumoroid and that covered by invadopodia. As the more densely packed non-invasive, propagating cells appear darker compared to invadopodia in a brightfield image (Figure 12A), this additional change in signal within the original mask allows placement of a secondary mask to exclude the invading areas of each tumoroid and separate the area covered by the two portions of the entire 3D structure (Figure 12). The area covered by invadopodia for U-87/fibroblast tumoroids increases dramatically over the seven day incubation period. LN-229/fibroblast tumoroids, by comparison, show little increase in invadopodia over the same time (Figure 12C). This dual analysis, therefore, has the potential to determine not only how rapidly tumoroid cells are propagating, but also the invasive nature of the cell model.

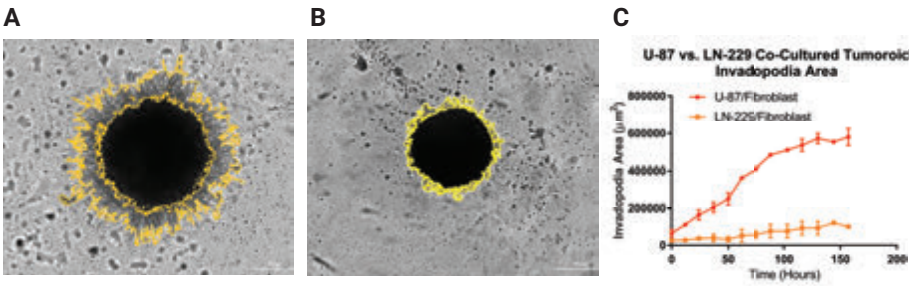

Figure 12. Kinetic uninhibited U-87 and LN-229 co-cultured tumoroid kinetic invadopodia areas. Calculated invadopodia area over time for non-treated U-87/fibroblast and LN-229/ fibroblast tumoroids. Invadopodia area calculated by the following formula: (Total AreaTime T – Non-Invading AreaTime T).

Recent publications using Agilent BioTek microscopes for monitoring 3D tumor necrosis

1. Kasper, S. H. et al. "Colorectal cancer-associated anaerobic bacteria proliferate in tumor spheroids and alter the microenvironment". *Sci. Rep. 10, 1–13,* **2020**.
2. Little, A. C. et al. "IL-4/IL-13 stimulated macrophages enhance breast cancer invasion via rho-GTPase regulation of synergistic VEGF/CCL-18 signaling". *Front. Oncol. 9, 1–13,* **2019**.

References

1. Uroz, M. et al. “Regulation of cell cycle progression by cell-cell and cell-matrix forces”. *Nat. Cell Biol. 20, 646–654,* **2018**.
2. Imamura, Y. et al. “Comparison of 2D- and 3D-culture models as drug-testing platforms in breast cancer”. *Oncol. Rep. 33, 1837–1843,* **2015**.
3. Fennema, E., Rivron, N., Rouwkema, J., van Blitterswijk, C. & De Boer, J. “Spheroid culture as a tool for creating 3D complex tissues”. *Trends Biotechnol. 31, 108–115,* **2013**.
4. Huh, D., Hamilton, G. A. & Ingber, D. E. “From 3D cell culture to organs-on-chips”. *Trends Cell Biol. 21, 745–754,* **2011**.
5. Tanner, K. & Gottesman, M. M. “Beyond 3D culture models of cancer”. *Sci. Transl. Med. 7, 1–5,* **2015**.
6. Edmondson, R., Broglie, J. J., Adcock, A. F. & Yang, L. “Three-dimensional cell culture systems and their applications in drug discovery and cell-based biosensors”. *Assay Drug Dev. Technol. 12, 207–218,* **2014**.
7. Langhans, S. A. “Three-dimensional *in vitro* cell culture models in drug discovery and drug repositioning”. *Front. Pharmacol. 9, 1–14,* **2018**.
8. Kasper, S. H. et al. “Colorectal cancer-associated anaerobic bacteria proliferate in tumor spheroids and alter the microenvironment”. *Sci. Rep. 10, 1–13,* **2020**.
9. Little, A. C. et al. “IL-4/IL-13 stimulated macrophages enhance breast cancer invasion via rho-GTPase regulation of synergistic VEGF/CCL-18 signaling”. *Front. Oncol. 9, 1–13,* **2019**.

Learn more:
www.agilent.com/lifesciences/biotek

Get answers to your technical questions and access resources in the Agilent Community:
community.agilent.com

Buy online:
www.agilent.com/chem/store

U.S. and Canada
1-800-227-9770
agilent_inquiries@agilent.com

Europe
info_agilent@agilent.com

Asia Pacific
inquiry_lsca@agilent.com

RA44173.6661574074

Published in the USA, February 1, 2021
5994-2571EN
AG091820_03

Agilent
Trusted Answers